Int. J. Electrochem. Sci., 13 **(2018)** 5860 – 5871, doi: 10.20964/2018.06.03

International Journal of
ELECTROCHEMICAL
SCIENCE
www.electrochemsci.org

Short Communication

Hierarchical Core-shell SnO_2/Ag/$Co(OH)_2$ Spheres Comprising Wrinkled Nanosheets for Highly Efficient Oxygen Evolution Reaction

Xin-Yu Zhang[1], *Jing-Qi Chi*[2], *Zi-Zhang Liu*[1], *Bin Dong*[1,2,*], *Yan-Ru Liu*[2], *Kai-Li Yan*[2], *Wen-Kun Gao*[1,2], *Yong-Ming Chai*[2], *Chen-Guang Liu*[2]

[1] College of Science, China University of Petroleum (East China), Qingdao 266580, PR China
[2] State Key Laboratory of Heavy Oil Processing, China University of Petroleum (East China), Qingdao 266580, PR China
[*]E-mail: dongbin@upc.edu.cn

Received: 21 July 2017 / *Accepted:* 13 September 2017 / *Published:* 10 May 2018

Hierarchical core-shell SnO_2/Ag/$Co(OH)_2$ spheres have been synthesized for efficient oxygen evolution reaction (OER) in alkaline solution using Ag-modified SnO_2 hollow spheres (SnO_2/Ag) as support. SnO_2/Ag hollow spheres can provide not only large surface area for the growth of $Co(OH)_2$ but also better conductivity and stability derived from Ag. XRD shows the formation of amorphous $Co(OH)_2$ supported on SnO_2/Ag. XPS confirms the existence and valence state of Sn, Ag and Co. EDX and SEM elemental mapping show the composition and good distribution of Sn, O, Ag and Co. SEM and TEM show that the wrinkled $Co(OH)_2$ nanosheets homogeneously covered on the surface of SnO_2/Ag hollow spheres, which implying more exposed active sites. OER measurements show that SnO_2/Ag/$Co(OH)_2$ has the enhanced performances with lower onset potential (1.4 V vs. RHE), smaller Tafel slope (80.04 mV dec^{-1}) than SnO_2/$Co(OH)_2$ and unsupported $Co(OH)_2$. Ag modification may be the key for enhancement performances for OER due to providing faster electron transfer rate. The excellent long-time stability of SnO_2/Ag/$Co(OH)_2$ may be ascribed to the close combination between $Co(OH)_2$ and SnO_2/Ag and stability of Ag in alkaline solution. The suitable support with good dispersion and conductivity can provide a facile way to prepare effective electrocatalysts for OER.

Keywords: SnO_2; Ag modification; $Co(OH)_2$; electrocatalyst; oxygen evolution reaction

1. INTRODUCTION

Electrolytic water splitting provides an effective pathway for global scale storage of renewable energy such as wind and solar in the form of hydrogen energy, enabling the continuous utilization of the intermittent energy sources [1-4]. There are two half reactions containing hydrogen evolution

reaction (HER) ($2H^+ + 2e^- \rightarrow H_2$) and oxygen evolution reaction (OER) ($2H_2O \rightarrow 4H^+ + O_2 + 4e^-$) in water splitting, which needs efficient electrocatalysts for both HER [5-10] and OER [11-16]. Especially, OER due to its complex transfer of four electrons, a relatively weak O-O bond and larger overpotentials during water splitting severely limits the enhancement of performance both in acidic and basic media [17-20]. Thus it is essential to develop highly efficient electrocatalysts to promote the OER. So far, noble metal oxides such as oxides of iridium (IrO_2) and ruthenium (RuO_2) have been widely probed to lower the energy barriers of OER so that hydrogen can be generated with appreciable rate at lower applied voltages [21-23]. However, the scarcity and high cost of noble metal based catalysts hinder their large scale application [24-26].

Recently, transition metal oxides or hydroxides composed of earth-abundant elements such as nickel oxide [27, 28] or cobalt hydroxides [29, 30] exhibit outstanding performance for oxygen evolution. Especially, cobalt hydroxides as a typical transition-metal layered materials with uniform edge-sharing octahedral transition metal oxide layers possess high electrocatalytic activity for OER due to the large surface area [31]. However, two-dimensional (2D) layered materials are extremely prone to stacking and aggregating due to the high surface energy and strong interlayer van der Waals forces, which may result in the decrease of active sites [32, 33]. Another disadvantage of cobalt hydroxides is the poor conductivity due to its semi-conductive nature, in which the electrons are tend to transfer along the layer structure of cobalt hydroxides nanosheets [34]. In regards to these problems, utilizing ideal support materials for host electrocatalysts has been continually emphasized because of their ability to yield the enhanced catalytic performances in electrochemical reactions [35]. Ideal supports can not only decrease the destructive agglomeration and provide high surface area to low the loading of catalysts but also possess excellent conductivity to accelerate the charge transfer rate [36]. In addition, the intimate contact of between active substance and the support are favorable for the stability of the catalysts [36]. Recently, many metal oxides such as CeO_2 [37], ZrO_2 [38] and SnO_2 [39] have been considered as ideal support due to unique nanostructures and excellent durability in both acid and basic electrolyte. Among these metal oxides supports, SnO_2 nanospheres with uniform hollow nanostructures have been considered as ideal candidates for enhanced electrocatalytic activities due to their specific surface area and surface permeability [40]. However, the poor conductivity of SnO_2 as support has been a limitation for further improving their electrocatalytic performance. Various strategies have been emphasized to improve the conductivity by taking advantage of doping metal as the conductive support [41]. Ag-modified materials have been widely searched because of the superior electron conductivity [42]. For example, Kim et al. synthesized amorphous α-$Co(OH)_2$ nanosheets grown on Ag nanowires with an overpotential of only 220 mV [43]. So we speculate that the poor conductivity of SnO_2 hollow spheres as supports can be improved by Ag-modification to further enhance the performance for HER.

Herein, we report a facile synthesis of $Co(OH)_2$ nanosheets anchored on the surface of SnO_2/Ag hollow spheres via a hydrolysis reaction at room temperature (Scheme 1). Firstly, uniform SnO_2 hollow nanospheres have been synthesized through a solvothermal method [44]. Then in order to enhance the conductivity of SnO_2 hollow nanospheres, a simple silver mirror reaction has been used to prepare Ag-modified SnO_2 nanospheres.

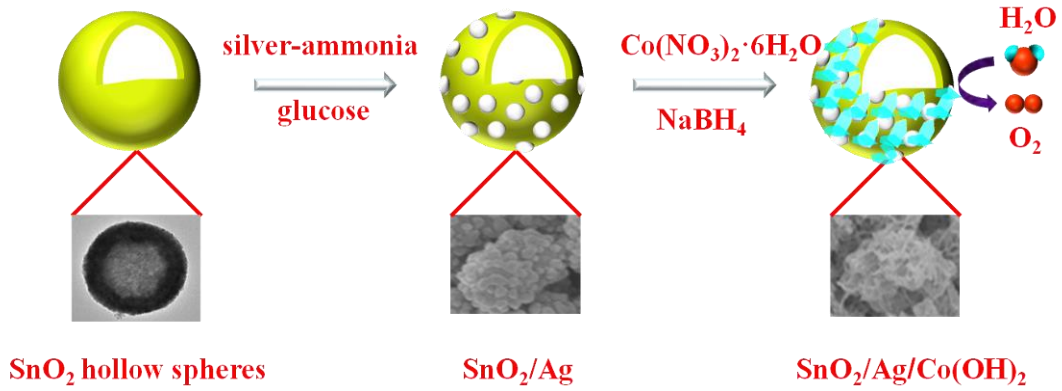

Scheme 1 Schematic representation of the synthesis procedures of core-shell SnO_2/Ag/$Co(OH)_2$.

Finally, wrinkled $Co(OH)_2$ nanosheets anchored on SnO_2/Ag have been achieved by a facile hydrolysis process. The modification of Ag with high conductivity is crucial for further improvement of the electrocatalytic performances of core-shell SnO_2/Ag/$Co(OH)_2$. The oxidation functional groups on the surface of SnO_2 hollow spheres also contributed to the close combination between $Co(OH)_2$ and the support. The electrochemical activity of SnO_2/Ag/$Co(OH)_2$ outperforms other samples reflected from lower overpotential of only 220 mV, smaller Tafel slope of 80 mV dec^{-1} and smaller charge-transfer resistance. Therefore, it can be concluded that Ag-modified SnO_2 nanospheres may be a better support for synthesizing $Co(OH)_2$ nanosheets for enhanced OER performances.

2. EXPERIMENTAL SECTION

2.1 Preparation of SnO_2 nanospheres and SnO_2/Ag/$Co(OH)_2$

All reagents were analytical grade and used without more purification. The synthesis of SnO_2 hollow nanospheres was carried out accordingly to previous reported [44]. In a typical synthesis process, 0.24 g of urea were dissolved in 40 mL of an ethanol/water ($v_{ethanol}$: v_{water}=3 : 5). Then 0.192 g of $K_2SnO_3{\cdot}3H_2O$ was added into the obtained solution under stirring about 10 min. Afterwards, the obtained translucent solution was transferred into 100 mL Teflon-lined stainless steel autoclave, keeping at 200°C for 20 h. After completion, the product was filtered and washed with deionized water and ethanol for three times, and then dried at 60 °C overnight.

For the synthesis of SnO_2/Ag nanospheres, 0.05 M $AgNO_3$ was dissolved in 20.0 mL deionized water and ammonium hydroxide solution (v_{NH3}: v_{H2O}=1 : 20) was added slowly until the solution become clear again forming silver-ammonia solution. Then 0.2g of synthesized SnO_2 hollow nanospheres was added into the obtained silver-ammonia solution with magnetic stirring for 30 min. Then 0.1 M glucose dissolved in 70 mL water was added. After a reaction at 75 °C for 1.5 h, the product was rinsed with water and ethanol for three times, and then dried in a vacuum oven.

The core-shell SnO_2/Ag/$Co(OH)_2$ was prepared through a facile room temperature reaction process. In a suspension consisting of 0.0493 g of SnO_2/Ag in 20 mL deionized water, 0.1903g $Co(NO_3)_2{\cdot}6H_2O$ were added, After a homogeneous solution was obtained under stirring, 1 ml water containing 0.06 g of $NaBH_4$ was injected into the reaction bath drop-wise at room temperature. After

stirring for 2 h, the obtained samples were collected through centrifugation and washed with water, and then dried at 60 °C for 8 h. For comparison, $Co(OH)_2$ and $SnO_2/Co(OH)_2$ were synthesized under the identical conditions with the absence of SnO_2/Ag and Ag, respectively.

2.2 Physical characterization

X-ray powder diffraction (XRD) (X'Pert PRO MPD, Cu KR) data of obtained samples were recorded with 2θ range from 10˚ to 70˚. X-ray photoelectron spectra (XPS) was performed on a spectrometer (Thermo Fisher Scientific II) using an Al Ka photon source to search the valence state of samples. Scanning electron microscopy (SEM, Hitachi, S-4800) analysis was applied to explore the morphology of obtained samples. Transmission electron microscopy (TEM) images were collected on JEM-2100UHR with an accelerating voltage of 200 kV. SEM elemental mapping and SEM X-ray fluorescence elemental analysis (EDX) were used to identify the main elements of the representative surface area of $SnO_2/Ag/Co(OH)_2$.

2.3 Electrochemical tests

All the electrochemical tests were carried out in a standard three-electrode cell with a catalyst-modified glassy carbon electrode (GCE) as work electrode, a Pt plate as a counter electrode, and a saturated calomel reference electrode (SCE) as reference electrode, respectively. For preparation of work electrode, typically, 5 mg of sample and 20 μL Nafion solution (5 wt%) were dissolved in 1 mL water-ethanol solution ($v_{ethanol}$: v_{water}=1 : 1) by sonicating for 0.5 h to form a homogeneous solution. Then 5 μL of the ink with the geometric area about 0.1256 cm^2 was loaded onto a glassy carbon electrode which was polished with alumina slurry. An O_2 purged 1 M KOH was used as the electrolyte for all the electrochemical tests. To evaluate the OER activity of obtained samples, linear sweep voltammetry (LSV) were performed with a scan rate of 10 mV s^{-1}. Electrochemical impedance spectroscopy (EIS) measurements were applied at 0.45 V (vs. SCE) with a frequency range from 100 KHz to 0.01 Hz by applying an AC voltage of 5 mV. In addition, cyclic voltammograms (CV) were used to evaluate the durability of sample from 0.45 V to 0.55 V (vs. SCE) at a scan rate of 100 mV s^{-1} for 500 times and 1000 times.

3. RESULTS AND DISCUSSION

Crystallographic properties of all the prepared samples are identified from XRD (Figure 1). For SnO_2 hollow spheres, main peaks at 26.5°, 33.8°, 37.9°, 51.7°, 54.7° and 61.7° can be attributed to the (110), (101), (200), (211), (220) and (310) planes of SnO_2 (PDF No. 01-077-0450), which shows that the peaks of the sample are consistent with the standard card of SnO_2 without other peaks from impurities. When Ag nanoparticles are coated on the surface of SnO_2 hollow spheres, the well-indexed diffraction peaks at 38.1°, 44.3° and 64.4° reveal the existence of metal Ag (PDF No. 00-004-0783). For $SnO_2/Ag/Co(OH)_2$, whereas peaks derived from $Co(OH)_2$ can't be observed in XRD patterns,

which may be due to the amorphous nature of $Co(OH)_2$. In addition, the intensity of peaks attributed to SnO_2 and Ag are weak compared with SnO_2/Ag mainly because of the coating of amorphous $Co(OH)_2$.

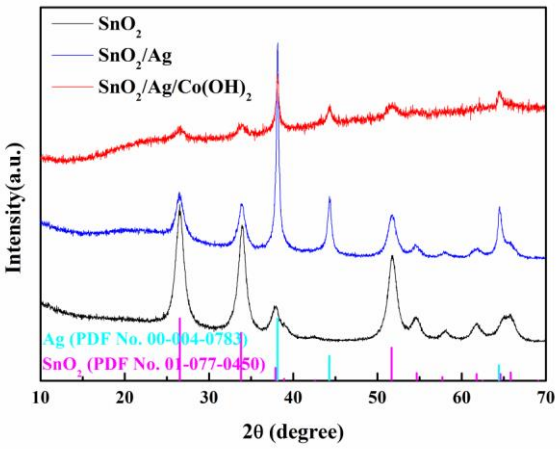

Figure 1. XRD patterns of all SnO_2, SnO_2/Ag and SnO_2/Ag/$Co(OH)_2$.

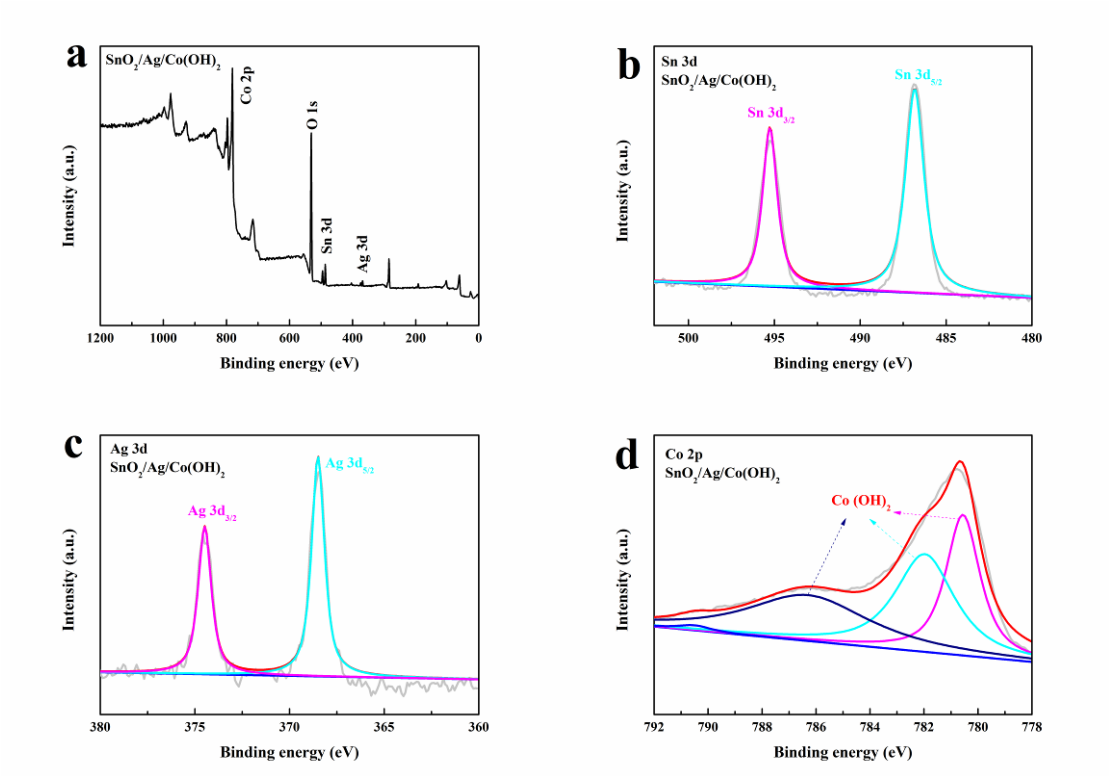

Figure 2. (a) XPS survey spectra for SnO_2/Ag/$Co(OH)_2$ in the (b) Sn 3d; (c) Ag 3d and (d) Co 2p regions.

In order to confirm the valence and composition of core-shell SnO_2/Ag/$Co(OH)_2$, XPS data are provided in Figure 2a-2d. As displayed in Figure 2a, the characteristic peaks of Sn, O, Ag and Co can be clearly observed in survey spectrum of SnO_2/Ag/$Co(OH)_2$. In Figure 2b, the peaks at 486.8 eV and 495.3 eV are assigned to Sn $3d_{5/2}$ [45] and Sn $3d_{3/2}$ [46], respectively, which are in good accordance

with the values for SnO_2. High resolution spectrum of Ag (Figure 2c) deriving from SnO_2/Ag/$Co(OH)_2$ shows that the peaks centered at 374.3 eV and 368.3 eV are attributed to Ag $3d_{3/2}$ and Ag $3d_{5/2}$, respectively [47]. In the Co 2p XPS spectrum (Figure 2d), the peaks at 780.6 eV, 782.4 eV, 786.2 eV and 790.6 eV are highly consistent with the curve-fitted Co $2p_{3/2}$ spectra for $Co(OH)_2$ [48, 49], confirming the composition of $Co(OH)_2$.

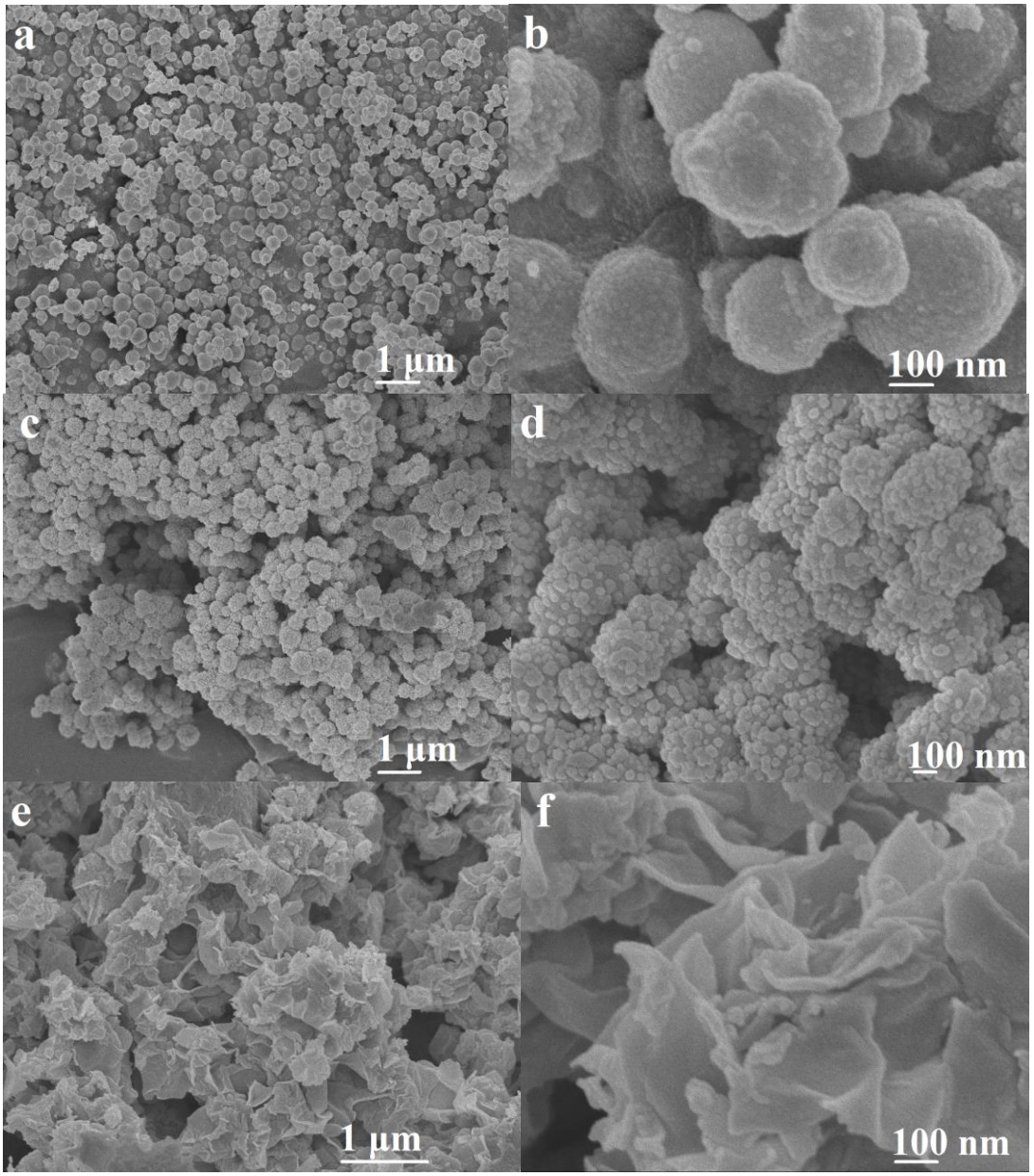

Figure 3. SEM images. (a,b) SnO_2 (c,d) SnO_2/Ag and (e,f) SnO_2/Ag/$Co(OH)_2$.

The morphology of the as-prepared samples including SnO_2, SnO_2/Ag, SnO_2/$Co(OH)_2$ and SnO_2/Ag/$Co(OH)_2$ are further investigated by SEM (Figure 3). As shown in Figure 3a and 3b, SnO_2 are homogeneously distributed hollow spheres with the diameter ranging from 200 to 400 nm.

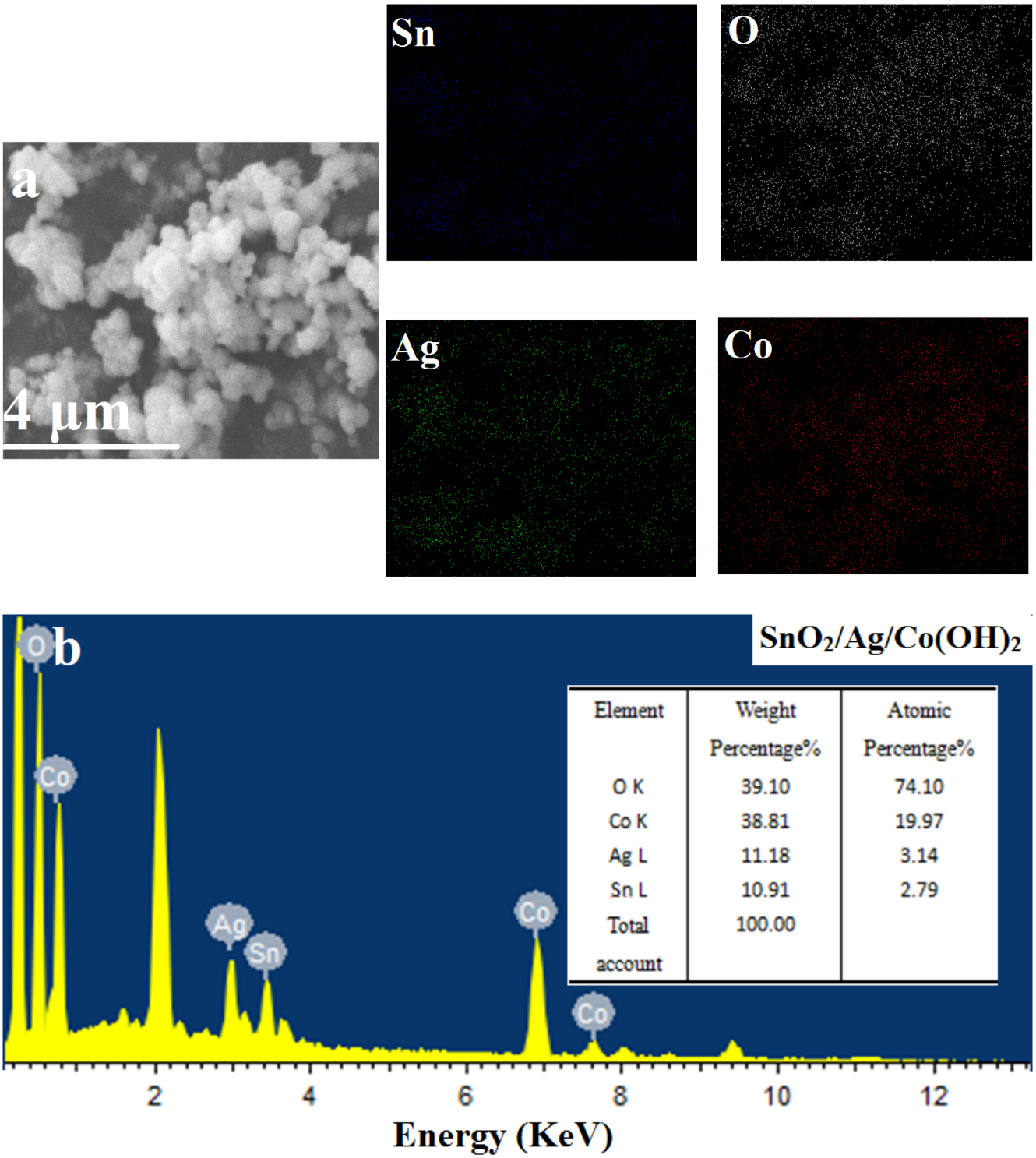

Figure 4. (a) SEM images and elemental mapping of SnO_2/Ag/$Co(OH)_2$ and (b) EDX of SnO_2/Ag/$Co(OH)_2$.

When SnO_2 was modified by Ag particles, the morphology of as-prepared SnO_2/Ag can be observed in Figure 3c and 3d. Figure 3c shows that SnO_2/Ag maintains the spherical morphology very well with rough surface. Under high magnification, Figure 3d reveals the surface of SnO_2 nanospheres are coated with uniform Ag nanoparticles. SEM images of SnO_2/Ag/$Co(OH)_2$ in Figure 3e reveal that

the surface of three-dimensional nanospheres of SnO_2/Ag has been entirely covered by uniform wrinkled $Co(OH)_2$ nanosheets with enhanced dispersion, implying larger surface area and more electrocatalytic active sites. A closer view in Figure 3f shows that wrinkled $Co(OH)_2$ nanosheets on SnO_2/Ag spheres can be clearly observed, which may provide more active sites for OER. In order to further confirm the existence and composition of elements, SEM and elemental mappings of SnO_2/Ag/$Co(OH)_2$ are shown in Figure 4. Figure 4a demonstrates the homogeneous distribution of Sn, O, Ag and Co elements. EDX data of SnO_2/Ag/$Co(OH)_2$ in Figure 4b also confirm the existence and composition of Sn, O, Ag and Co elements. The more clear monodispersed morphology of SnO_2 and SnO_2/Ag/$Co(OH)_2$ hollow nanospheres has been characterized by TEM in Figure 5. As shown in Figure 5a and 5b, uniform SnO_2 hollow spheres with the diameter ranging from 200 to 400 nm are monodispersed state, which is identical with SEM results. TEM images of core-shell SnO_2/Ag/$Co(OH)_2$ can be observed in Figure 5c and 5d. Compared with the pure SnO_2 hollow nanospheres, core-shell SnO_2/Ag/$Co(OH)_2$ maintains the spherical morphology well with very thin film coating, which may lead to larger surface area and expose more electrocatalytic active sites. TEM images show that $Co(OH)_2$ nanosheets can well anchor and disperse on the surface of SnO_2/Ag nanospheres.

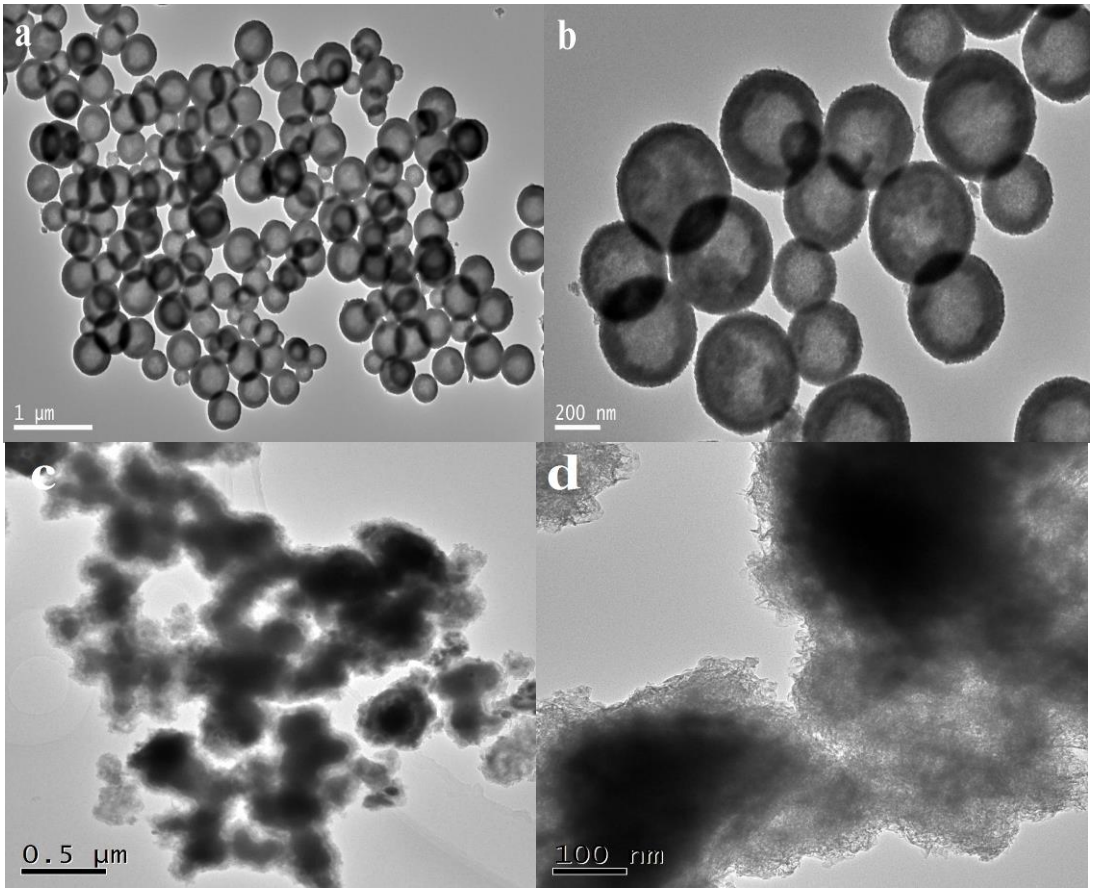

Figure 5. TEM image. (a,b) SnO_2 and (c,d) SnO_2/Ag/$Co(OH)_2$.

Figure 6 shows OER measurements of all the five samples including SnO_2, SnO_2/Ag, $Co(OH)_2$, SnO_2/$Co(OH)_2$ and SnO_2/Ag/$Co(OH)_2$. Figure 6a shows LSV curves of all the samples. It can be seen

that $SnO_2/Ag/Co(OH)_2$ possess lower onset potential of 170 mV and an overpotential of 340 mV to reach 10 mA cm^{-2}. The low overpotential of $SnO_2/Ag/Co(OH)_2$ compare favorably to some of reported non-noble-metal OER electrocatalysts in alkaline solution, such as $Co_3V_2O_8$ ($\eta_{10\ mA\ cm^{-2}}$=359 mV, 1.0 M KOH) [50], mesoporous Co_3O_4 ($\eta_{10\ mA\ cm^{-2}}$=411 mV, 1.0 M KOH) [51], CoCo-NS ($\eta_{10\ mA\ cm^{-2}}$=350 mV, 1.0 M KOH) [52]. A more detailed comparison is listed in Table 1. Meanwhile, SnO_2 and SnO_2/Ag possess no obvious current density demonstrating that both Ag and SnO_2 are not active sites for OER while the doping of Ag contributes to the enhanced activity by improving the conductivity of active sites. Furthermore, $SnO_2/Co(OH)_2$ has a lower onset potential (1.5 V vs. RHE) than pure $Co(OH)_2$ with an onset potential of (1.55 V vs. RHE) indicating that enhanced OER performance can be achieved by utilizing support to improve the dispersion of $Co(OH)_2$. In agreement with LSV results, Tafel slope of $SnO_2/Ag/Co(OH)_2$ (80.04 mV dec^{-1}) is much smaller than that of $SnO_2/Co(OH)_2$ (83.37 mV dec^{-1}), SnO_2/Ag (187.78 mV dec^{-1}), $Co(OH)_2$ (216 mV dec^{-1}) and SnO_2 (288.78 mV dec^{-1}) as shown in Figure 6b, indicating faster kinetics of $Ag/SnO_2/Co(OH)_2$ for OER. The enhanced electrocatalytic performances of $Ag/SnO_2/Co(OH)_2$ with low overpotential and faster kinetics could be ascribed to the synergistic effect among catalytic active $Co(OH)_2$ and excellent conductivity of SnO2 with Ag-modification.

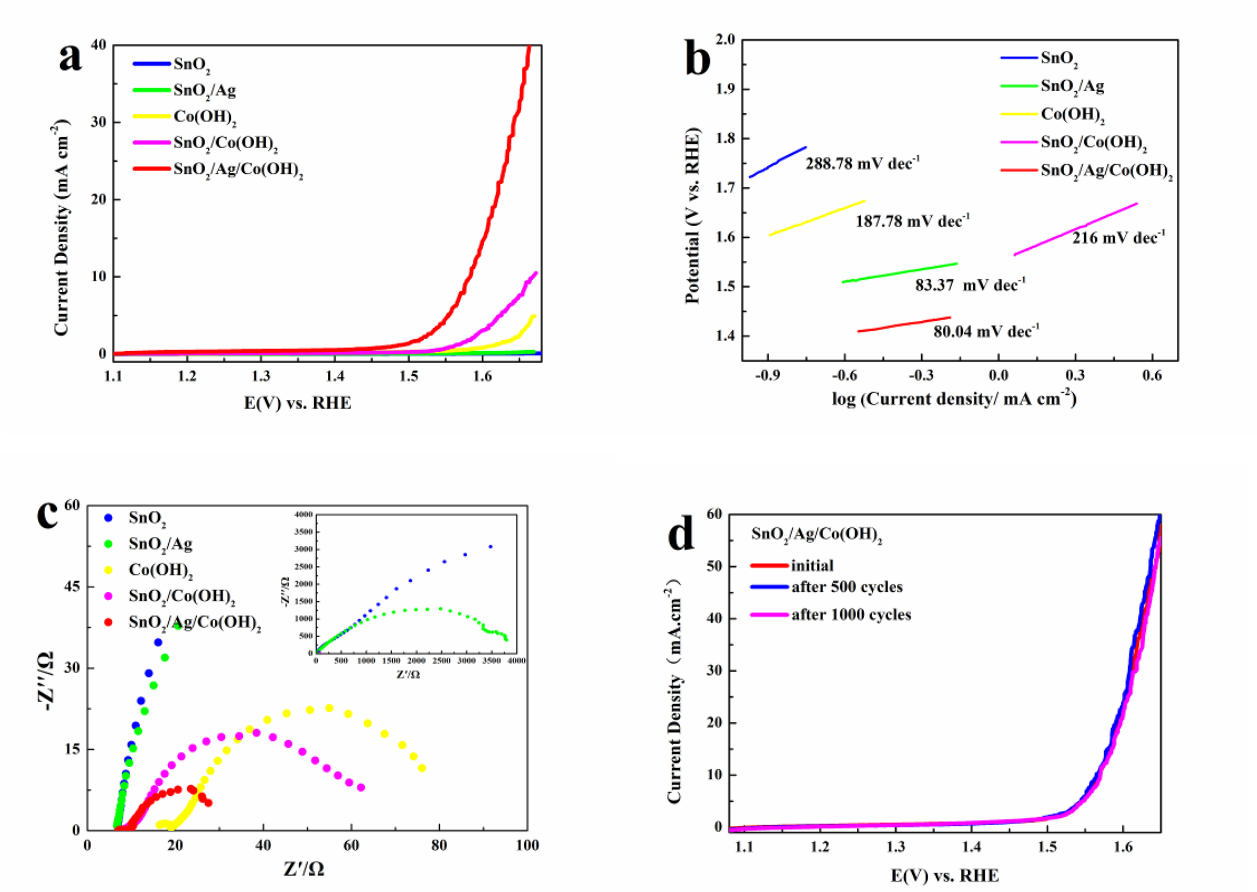

Figure 6. (a) Comparison of LSV curves on SnO_2, SnO_2/Ag, $Co(OH)_2$, $SnO_2/Co(OH)_2$ and $SnO_2/Ag/Co(OH)_2$ at a scan rate of 10 mV s^{-1}in 1.0 M KOH. (b) Corresponding Tafel plots extracted from panel a. (c) Nyquist plots of SnO_2, SnO_2/Ag, $Co(OH)_2$, $SnO_2/Co(OH)_2$ and $SnO_2/Ag/Co(OH)_2$ at 0.45 V (vs. SCE) from 10^5 to 0.01 Hz. (d) Polarization curves of $SnO_2/Ag/Co(OH)_2$ before and after 500 and 1000 cycles used for stability tests.

In addition, electrochemical impedance spectroscopy (EIS) measurements are performed on the obtained catalysts to observe charge transport behaviour (Figure 6c). A charge transport resistance (R_{ct}), associated with the diameter of the semicircle displayed in the high frequency of a Nyquist plot, represents the electron conductivity of the catalyst. Compared with other samples especially $SnO_2/Co(OH)_2$, $SnO_2/Ag/Co(OH)_2$ exhibits smallest semicircle in the Nyquist plot, meaning lowest charge transfer resistance due to coating of Ag nanoparticles. The decreasing R_{ct} value indicates that charge transport rate can be promoted by the intimate connection between active sites and the conductive SnO_2/Ag support. Figure 6d demonstrates the polarization curves of $Ag/SnO_2/Co(OH)_2$ measured before, after 500 CV circles and after 1000 CV circles. The LSV curve remains nearly unchanged with only negligible loss of the current. The main reason for the degradation may be attributed to structural deformations and the diffusion of the produced O_2 bubbles on the surface of eletrocatalysts.

Table 1. Comparison of OER activity of $SnO_2/Ag/Co(OH)_2$ with the reported non-noble-metal electrocatalysts in alkaline solution.

Electrocatalyst	E_{10} (V vs. RHE) (mV)	b (mV dec^{-1})	Electrolyte solution	Ref.
$SnO_2/Ag/Co(OH)_2$	340	80.04	1.0 M KOH	This work
$Co_3V_2O_8$	359	65	1.0 M KOH	50
Co_3O_4	384	72	1.0 M KOH	50
V_2O_5	451	85	1.0 M KOH	50
Mesoporous Co_3O_4	411	80	0.1 M KOH	51
CoCo-NS	350	45	1.0 M KOH	52
$NiCo_2O_4$/graphene	500	161	0.1 M KOH	53
CoO/CNT	550	108	1.0 M KOH	54
Co-S/Ti mesh	361	64	1.0 M KOH	55

4. CONLUSIONS

In this work, $Co(OH)_2$ nanosheets anchored on high conductive Ag-modified SnO_2 hollow spheres could be successfully synthesized via a facile hydrolysis reaction at room temperature. By introducing Ag-modified SnO_2 spheres as support, the onset potential is negatively shifted by 100 mV comparing with those of the unsupported $Co(OH)_2$. The enhanced electrocatalytic performances could be ascribed to the large surface area and faster electron transport due to Ag modification and wrinkled $Co(OH)_2$ nanosheets. SnO_2/Ag hollow spheres may be a good support for efficient OER activity electrocatalysts.

ACKNOWLEDGEMENTS
This work is financially supported by the Fundamental Research Funds for the Central Universities (15CX05031A) and National Training Program of Innovation and Entrepreneurship for Undergraduates (No. 201610425061).

References

1. X. H. Lu, S. Xie, H. Yang, Y. Tong and H. B. Ji, *Chem. Soc. Rev.*, 43 (2014) 7581.
2. Y. R. Liu, W. H. Hu, X. Li, B. Dong, X. Shang, G. Q. Han, Y. M. Chai, Y. Q. Liu and C. G. Liu, *Appl. Surf. Sci.*, 384 (2016) 51.
3. X. X. Zou and Y. Zhang, *Chem. Soc. Rev.*, 44 (2015) 5148.
4. W. H. Hu, R. Yu, G. Q. Han, Y. R. Liu, B. Dong, Y. M. Chai, Y. Q. Liu and C. G. Liu, *Mater. Lett.*, 161 (2015) 120.
5. J. X. Feng, H. Xu, Y. T. Dong, X. F. Lu, Y. X. Tong and G. R. Li, *Angew. Chem. Int. Ed.*, 56 (2017) 1.
6. X. Shang, W. H. Hu, X. Li, B. Dong, Y. R. Liu, G. Q. Han, Y. M. Chai and C. G. Liu, *Electrochim. Acta*, 224 (2017) 25.
7. W. H. Hu, X. Shang, J. Xue, B. Dong, J. Q. Chi, G. Q. Han, Y. R. Liu, X. Li, K. L. Yan, Y. M. Chai and C. G. Liu, *Int. J. Hydrogen Energy*, 42 (2017) 2088.
8. M. Fan, R. Gao, Y. C. Zou, D. Wang, N. Bai, G. D. Li and X. X. Zou, *Electrochim. Acta*, 215 (2016) 366.
9. Y. R. Liu, X. Shang, W. K. Gao, B. Dong, X. Li, X. H. Li, J. C. Zhao, Y. M. Chai, Y. Q. Liu and C. G. Liu, *J. Mater. Chem. A*, 5 (2017) 2885.
10. G. Q. Han, X. Li, J. Xue, B. Dong, X. Shang, W. H. Hu, Y. R. Liu, J. Q. Chi, K. L. Yan, Y. M. Chai and C. G. Liu, *Int. J. Hydrogen Energy*, 42 (2017) 2952.
11. B. Y. Xia, Y. Yan, N. Li, H. B. Wu, X. W. Lou and X. Wang, *Nat. Energy*, 1 (2016) 15006.
12. T. Liu, A.M. Asiri and X. Sun, *Nanoscale*, 8 (2016) 3911.
13. L. Wang, A. Ambrosi and M. Pumera, *Angew. Chem. Int. Ed.*, 52 (2013) 13818.
14. X. Li, G. Q. Han, Y. R. Liu, B. Dong, W. H. Hu, X. Shang, Y. M. Chai and C. G. Liu, *ACS Applied Materials & Interfaces*, 8 (2016) 20057.
15. J. Q. Chi, X. Shang, F. Liang, B. Dong, X. Li, Y. R. Liu, K. L. Yan, W. K. Gao, Y. M. Chai and C. G. Liu, *Appl. Surf. Sci.*, 401 (2017) 17.
16. X. Li, G.Q. Han, Y.R. Liu, B. Dong, X. Shang, W.H. Hu, Y.M. Chai, Y.Q. Liu and C.G. Liu, *Electrochim. Acta*, 205 (2016) 77.
17. S. W. Li, S. J. Peng, L. S. Huang, X. Q. Cui, A. M. Al-Enizi and G. Zheng, *ACS Appl. Mater. Interfaces*, 8 (2016) 20534.
18. B. Dong, X. Zhao, G. Q. Han, X. Li, X. Shang, Y. R. Liu, W. H. Hu, Y. M. Chai, H. Zhao and C. G. Liu, *J. Mater. Chem. A*, 4 (2016) 13499.
19. C. Xie, Y. Wang, K. Hu, L. Tao, X. Huang, J. Huo and S. Y. Wang, *J. Mater. Chem. A*, 5 (2017) 87.
20. X. Li, X. Shang, Y. Rao, B. Dong, G. Q. Han, W. H. Hu, Y. R. Liu, K. L. Yan, J. Q. Chi, Y. M. Chai and C. G. Liu, *Appl. Surf. Sci.*, 396 (2017) 1034.
21. T. Liu, Y. Liang, Q. Liu, X. Sun, Y. He and A.M. Asiri, *Electrochem. Commun.*, 60 (2015) 92.
22. X. F. Lu, L. F. Gu, J. W. Wang, J. X. Wu, P. Q. Liao and G. R. Li, *Adv. Mater.*, 29 (2017) 1604437
23. X. Zhao, X. Shang, Y. Quan, B. Dong, G. Q. Han, X. Li, Y. R. Liu, Q. Chen, Y. M. Chai and C. G. Liu, *Electrochim. Acta*, 230 (2017) 151.
24. X. Shang, K. L. Yan, Y. Rao, B. Dong, J. Q. Chi, Y. R. Liu, X. Li, Y. M. Chai and C. G. Liu, *Nanoscale*, (2017) DOI: 10.1039/C7NR02867A
25. C. C. L. McCrory, S. Jung, J. C. Peters and T. F. Jaramillo, *J. Am. Chem. Soc.*, 135 (2013) 16977.
26. B. Dong, W. H. Hu, G. Q. Han, Y. M. Chai and C. G. Liu, *Materials Review*, 30 (8A) (2016) 39.
27. D. A. Corrigan and R. M. Bendert, *J. Electrochem. Soc.*, 136 (1989) 723.
28. G. Q. Han, Y. R. Liu, W. H. Hu, B. Dong, X. Li, X. Shang, Y. M. Chai, Y. Q. Liu and C. G. Liu, *Appl. Surf. Sci.*, 359 (2015) 172.
29. J. X. Feng, H. Xu, Y. T. Dong, S. H. Ye, Y. X. Tong and G. R. Li, *Angew. Chem. Int. Ed.*, 55 (2016) 3694.

30. J. Li, Y. Wang, T. Zhou, H. Zhang, X. Sun, J. Tang, L. Zhang, A.M. Al-Enizi, Z. Yang and G. Zheng, *J. Am. Chem. Soc.*, 137 (2015) 14305.
31. M. Gong and H. Dai, *Nano Res.*, 8 (2015) 23.
32. W. H. Hu, G. Q. Han, Y. R. Liu, B. Dong, Y. M. Chai, Y. Q. Liu and C. G. Liu, *Int. J. Hydrogen Energy*, 40 (2015) 6552.
33. A.A. Jeffery, C. Nethravathi and M. Rajamathi, *J. Phys. Chem. C*, 118 (2014) 1386.
34. X. Long, S. Xiao, Z. Wang, X. Zheng and S. Yang, *Chem. Commun.*, 51 (2015) 1120.
35. C.M.A. Parlett, D.W. Bruce, N.S. Hondow, A.F. Lee and K. Wilson, *ACS Catal.* 1 (2011) 636.
36. J.H. Kim, J.Y. Cheon, T.J. Shin, J.Y. Park and S.H. Joo, *Carbon* 101 (2016) 449.
37. J. X. Feng, S. H. Ye, H. Xu, Y. X. Tong and G. R. Li, *Adv. Mater.*, 28 (2016) 4698.
38. T.H. Yeh and C.C. Chou, *J. Phys. Chem. Solids*, 69 (2008) 386.
39. B. Zhao, X. Guo, W. Zhao, J. Deng, G. Shao, B. Fan, Z. Bai and R. Zhang, *ACS Appl. Mater. Interfaces*, 8 (2016) 28917.
40. T. Zhu, Z.Y. Wang, S.J. Ding, J.S. Chen and X.W. Lou, *RSC Adv.*,1 (2011) 397.
41. R.D.L. Smith, M.S. Prevot, R.D. Fagan, S. Trudel and C.P. Berlinguette, *J. Am. Chem. Soc.*, 135 (2013) 11580.
42. E. Baran and B. Yazici, *Int. J. Hydrogen Energy*, 41 (2016) 2498.
43. H. Kim, Y. Kim, Y. Noh and W. Kim, *Dalton Trans.*, 45 (2016) 13686.
44. C.F. Zhang, H.B. Wu, C.Z. Yuan, Z.P. Guo and X.W. Lou, *Angew. Chem. Int. Ed.*, 124 (2012) 9730.
45. H. Shan, C. Liu, L. Liu, J. Zhang, H. Li, Z. Liu, X. Zhang, X. Bo and X. Chi, *ACS Appl. Mater. Interfaces*, 5 (2013) 6376.
46. L. Liu, S. Li, L. Wang, C. Guo, Q. Dong and W. Li, *J. Am. Ceram. Soc.*, 94 (2011) 771.
47. I. Lopez-Salido, D.C. Lim and Y.D. Kim, *Surface Science*, 588 (2005) 6.
48. J. Yang, H. Liu, W.N. Martens and R.L. Frost, *J. Phys. Chem. C*, 114 (2009) 111.
49. K. Artyushkova, S. Levendosky, P. Atanassov and J. Fulghum, *J. Top.Catal.*, 46 (2007) 263.
50. M. Xing, L. Kong, M. Liu, L. Liu, L. Kang and Y. Luo, J. Mater. Chem. A, 2 (2014) 18435.
51. Y. J. Sa, K. Kwon, J. Y. Cheon, J. Y. Cheon, F. Kleitz and S. H. Joo, J. Mater. Chem. A, 1 (2013) 9992.
52. F. Song and X. Hu, Nat. Commun., 5 (2014) 4477.
53. D. U. Lee, B. J. Kim and Z. W. Chen, J. Mater. Chem. A, 1 (2013) 4754 .
54. J. Wu, Y. Xue, X. Yan, W. Yan, Q. Cheng and Y. Xie, Nano Res., 5 (2012) 521.
55. T. Liu, Y. Liang, Q. Liu, X. Sun, Y. He, A.M. Asiri, Electrochem. Commun., 60 (2015) 92.